Persson, E., Selander, M., Linse, S., Drakenberg, T., Öhlin, A.-K., & Stenflo, J. (1989) *J. Biol. Chem. 264*, 16897-16904.
Scheek, R. M., van Gunsteren, W. F., & Kaptein, R. (1989) *Methods Enzymol. 177*, 204-218.
Selander, M., Persson, E., Stenflo, J., & Drakenberg, T. (1990) *Biochemistry 29*, 8111-8118.
Selander, M., Ullner, M., Persson, E., Teleman, O., Stenflo, J., & Drakenberg, T. (1992) *J. Biol. Chem.* (in press).
Stenflo, J. (1991) *Blood 78*, 1637-1651.
Stenflo, J., Lundvall, Å., Dahlbäck, B. (1987) *Proc. Natl. Acad. Sci. U.S.A. 84*, 368.
Teleman, O., & Jönsson, B. (1987) *J. Comput. Chem. 6*, 58-66.
Todaro, G. T., Fryling, C. & DeLarco, J. E. (1990) *Proc. Natl. Acad. Sci. U.S.A. 77*, 5258-5262.
Wagner, G., Braun, W., Havel, T. F., Schaumann, T., Go, N., & Wüthrich, K. (1987) *J. Mol. Biol. 196*, 611-639.
Williamsson, M. P., Havel, T. F., & Wüthrich, K. (1985) *J. Mol. Biol. 182*, 295-315.
Wüthrich, K. (1986) *NMR of Proteins and Nucleic Acids*, Wiley, New York.
Wüthrich, K., Billeter, M., & Braun, W. (1983) *J. Mol. Biol. 169*, 949-961.

Surface Binding Kinetics of Prothrombin Fragment 1 on Planar Membranes Measured by Total Internal Reflection Fluorescence Microscopy†

Kenneth H. Pearce, Richard G. Hiskey, and Nancy L. Thompson*
Department of Chemistry, University of North Carolina, Chapel Hill, North Carolina 27599
Received November 13, 1991; Revised Manuscript Received April 14, 1992

ABSTRACT: Total internal reflection fluorescence microscopy (TIRFM) has been employed to investigate the Ca^{2+}-dependent membrane-binding characteristics of fluorescein-labeled bovine prothrombin fragment 1 (F-BF1). Light scattering measurements demonstrated that F-BF1 bound to small unilamellar phosphatidylserine/phosphatidylcholine (25/75, mol/mol) vesicles with an apparent dissociation constant (1.5 ± 0.2 μM) similar to that of unlabeled protein (1.1 ± 0.1 μM). Negatively charged supported planar membranes were constructed by fusing small unilamellar vesicles at quartz surfaces. TIRFM measurements under equilibrium conditions showed that F-BF1 bound to planar membranes with an apparent dissociation constant (0.9 ± 0.2 μM) approximately equal to that on vesicles. Total internal reflection/fluorescence photobleaching recovery (TIR/FPR) curves for F-BF1 on 25 mol % PS planar surfaces were diffusion-influenced at F-BF1 solution concentrations ≤5 μM. Fluorescence recovery rates from samples of high F-BF1 concentrations were slowed by increasing the solution viscosity with glycerol, thus providing further support for a diffusion-limited effect at low F-BF1 concentrations. Analysis of the reaction-limited fluorescence recovery curves at F-BF1 solution concentrations ≥10 μM gave average association and dissociation kinetic rates of $\approx 10^5$ M^{-1} s^{-1} and ≈0.1 s^{-1}, respectively. Kinetic association rates increased significantly with increasing PS, whereas kinetic dissociation rates increased only slightly. Fluorescence recovery curves were nonmonoexponential; possible mechanisms for this behavior are described.

Upon vascular damage, the intrinsic and extrinsic pathways of the blood coagulation cascade converge into a common set of reactions to produce an assembled prothrombinase complex (Jackson & Nemerson, 1980; Mann et al., 1988). A central process in the formation of a fibrin clot is the surface-dependent catalytic conversion of the zymogen, prothrombin, to the active serine protease, thrombin, by prothrombinase (Mann et al., 1990). This enzyme complex is composed of factor X_a, a serine protease, factor V_a, a protein cofactor, and Ca^{2+} assembled on membrane surfaces containing negatively charged phospholipids, such as endothelial cell walls, blood platelets, monocytes, and lymphocytes. Even though thrombin production can occur at slow rates in solution, the localization of prothrombin and the prothrombinase proteins on a membrane surface is required for physiologically relevant activity (Mann et al., 1990). It has been suggested that exposure of negatively charged phospholipids in certain cell types is an event critical in providing a macroscopic surface for the assembly of many blood coagulation proteins. In resting-state platelets, for example, acidic lipids are primarily localized to the inner leaflet. Prothrombin-converting activity by stimulated platelets is greatly enhanced as accompanied by exposure of a procoagulant surface consisting of approximately 25 mol % phosphatidylserine to the membrane exterior (Bevers et al., 1982; Rosing et al., 1985).

To sustain membrane-binding capabilities, several of the factors involved in initiation and regulation of the blood clotting cascade, such as prothrombin, require a vitamin K-dependent posttranslational modification in which glutamic acid is converted to γ-carboxyglutamic acid (Gla). Each of the vitamin K-dependent proteins has a highly homologous amino-terminal domain containing 9–12 γ-carboxyglutamic acid residues (Furie & Furie, 1988). It is presently accepted, in the case of prothrombin, that membrane binding is in part due to electrostatic interactions. One model suggests that Ca^{2+} bridges negatively charged Gla residues to acidic phospholipids, resulting in a reversible, nonpenetrating prothrombin–membrane association. Prothrombin fragment 1, the amino-ter-

† This work was supported by National Science Foundation Grant DCB-8552986 (N.L.T.), a Teacher-Scholar Award from the Camille and Henry Dreyfus Foundation (N.L.T.), and National Institute of Health Grant HL-20161 (R.G.H.).
* To whom correspondence should be addressed.

0006-2960/92/0431-5983$03.00/0

minal 156 amino acid portion of prothrombin containing the Gla domain and a kringle structure, has membrane-binding characteristics similar to those of intact prothrombin (Dombrose et al., 1979).

One method of characterizing the association of extrinsic proteins with membranes, such as fragment 1 on acidic phospholipid surfaces, is to use total internal reflection fluorescence microscopy (TIRFM)[1] (Axelrod et al., 1984; Thompson et al., 1988). In this technique, an incident laser beam is internally reflected at a solid/liquid interface, which creates a thin layer of surface illumination termed the evanescent field. This penetration of light into solution allows for the selective excitation of fluorescent, surface-bound molecules. For the study of proteins at membrane surfaces using TIRFM, planar models of cell membranes can be constructed by depositing lipid layers on transparent quartz substrates. TIRFM has previously been used to investigate receptor–ligand interactions (Watts et al., 1986; Poglitsch et al., 1991), molecular orientations of fluorescent lipids in phospholipid monolayers (Timbs & Thompson, 1990), equilibrium binding characteristics of proteins at planar surfaces (Pisarchick & Thompson, 1990; Tendian et al., 1991), and cell-surface contact regions (Nakache et al., 1986).

Total internal reflection coupled with fluorescence photobleaching recovery (TIR/FPR) (Thompson et al., 1981) can be used to obtain surface binding kinetics of proteins at planar surfaces. A quick pulse of laser light irreversibly photobleaches a portion of the surface-bound fluorescent molecules in the evanescent wave. Fluorescence recovery, monitored by a much less intense beam, occurs as bleached molecules exchange with those in solution. Therefore, if fluorescence recovery is not dominated by the rates of solution transport or surface diffusion, quantitative information concerning the intrinsic binding rates of the protein at the surface can be obtained. TIR/FPR has previously been used to examine the dynamics of bovine serum albumin on quartz and polymer-coated quartz (Burghardt & Axelrod, 1981; Tilton et al., 1990a,b; Zimmerman et al., 1990), the adsorption of lysozyme on a hydrophobic surface (Schmidt et al., 1990), and the kinetics of epidermal growth factor binding to cell membrane surfaces (Hellen & Axelrod, 1991).

An understanding of the dynamics of prothrombin and the prothrombinase complex at membrane surfaces is essential for a complete understanding of the mechanism of thrombin production and subsequent blood coagulation. To develop a description of the role of the membrane in the assembly of prothrombinase and in substrate delivery to the complex, it is necessary to quantitatively define binding parameters at the solution/membrane interface. Past studies have used 90° light scattering (Nelsestuen & Broderius, 1977; Nelsestuen & Lim, 1977; Wei et al., 1982), surface pressure measurements (Mayer et al., 1983), and ellipsometry (Cuypers et al., 1983; Kop et al., 1984; Corsel et al., 1986) to characterize the Ca^{2+}-specific association of prothrombin, fragment 1, and other blood coagulation proteins with acidic membranes. The present work concerns the application of a recently developed technique in laser-based fluorescence microscopy (TIR/FPR) to investigate the membrane binding kinetics of bovine prothrombin fragment 1 (BF1) with model coagulation surfaces.

[1] Abbreviations: BF1, bovine prothrombin fragment 1; Gla, γ-carboxyglutamic acid; Na_2EDTA, disodium ethylenediaminetetraacetate; TIRFM, total internal reflection fluorescence microscopy; TIR/FPR, total internal reflection/fluorescence photobleaching recovery; F-BF1, fluorescein–bovine fragment 1; FITC, fluorescein-5-isothiocyanate; POPC, 1-palmitoyl-2-oleoyl-*sn*-glycero-3-phosphocholine; PS, bovine brain phosphatidylserine; NBD-PC, 1-acyl-2-[12-[(7-nitro-2-1,3,benzoxadiazol-4-yl)amino]dodecanoyl]-*sn*-glycero-3-phosphocholine.

Materials and Methods

Preparation of Prothrombin Fragment 1. Bovine prothrombin was isolated from plasma and purified according to the method of Mann (1977). BF1 was obtained by digestion of prothrombin with ecarin snake venom (Sigma Chemical Co., St. Louis, MO) as described (Pollock et al., 1988) and stored at −70 °C until use. The purity and molecular weight (23 500) of BF1 preparations were verified by reducing SDS–PAGE and the Gelcode silver stain procedure (Pierce Chemical Co., Rockford, IL). Protein concentration was determined by optical density using ϵ_{280} = 1.05 mL mg^{-1} cm^{-1} (Mann, 1977). All preparations exhibited a 42–50% quenching of tryptophan fluorescence upon addition of 10 mM $CaCl_2$ (Nelsestuen, 1976; Prendergast & Mann, 1977).

Fluorescence Labeling. BF1 samples (0.2 mg/mL) were equilibrated by dialysis with 0.05 M $NaHCO_3$ and 1 mM Na_2EDTA, pH 9.0, in preparation for the labeling procedure (Mishell & Shiigi, 1980). A 150-fold molar excess of fluorescein isothiocyanate isomer 1 (FITC; Molecular Probes, Inc., Junction City, OR) was dissolved in a volume of *N,N*-dimethylformamide (DMF) 100-fold lower than the volume of protein solution. The FITC/DMF solution was added dropwise to the protein solution, and the mixture was incubated at room temperature for 1 h. The labeled protein (F-BF1) was separated from unreacted dye by chromatography on Sephadex G-25 and exhaustive dialysis against Tris buffer (0.05 M Tris, 0.1 M NaCl, pH 7.4). Illumination of samples on SDS–PAGE by ultraviolet light showed the F-BF1 samples to be free of unreacted dye.

Determination of the concentration of F-BF1 by optical density was complicated by the absorbance of the conjugated fluorescein; therefore, the concentration of labeled protein was determined by the bicinchoninic acid (BCA) assay (Pierce, Rockford, IL). The accuracy of this assay was verified by comparison to concentrations obtained by sulfhydryl determination (Habeeb, 1972) using Ellman's reagent. Molar ratios of fluorescein to BF1 (1.2–0.5) were determined using the molar absorbtivity, ϵ_{494} = 64 800 L mol^{-1} cm^{-1} (Molecular Probes), for protein-conjugated fluorescein. Samples of F-BF1 were stored at −70 °C and thawed immediately before use.

The viability of F-BF1 was partially confirmed by the ability of Ca^{2+} to induce biphasic tryptophan fluorescence quenching. F-BF1 exhibited an intrinsic fluorescence quench (28–35%) similar to that of unlabeled protein. The emission of BF1-conjugated fluorescein was monitored to investigate the effect of $CaCl_2$ and vesicles on the fluorescein fluorescence. Solutions contained 0.025 mg/mL F-BF1 with or without 10 mM $CaCl_2$ and/or 0.05 mg/mL PS/POPC vesicles (25/75, mol/mol) in Tris buffer.

Phospholipid Vesicles. Aliquots of bovine brain sodium salt phosphatidylserine (PS) and 1-palmitoyl-2-oleoyl-*sn*-glycero-3-phosphocholine (POPC) (Avanti Polar Lipids, Birmingham, AL) in chloroform were combined, dried under a stream of nitrogen to a thin film, redissolved in 1 mL of cyclohexane, dried by vacuum centrifugation, and then resuspended to 2 mM with Tris buffer. The lipid mixture was sonicated (Artek Systems sonic dismembrator model 300, Farmingdale, NY) to clarity with ~2-min pulses for a total of ~30 min and then fractionated by centrifuging for 20 min at 130000*g* in an air ultracentrifuge (Beckman Instruments, Palo Alto, CA). The top half of the centrifuged vesicle suspension was used within 24 h. In some cases, 1-acyl-2-[12-[(7-nitro-2-1,3-benzoxadiazol-4-yl)amino]dodecanoyl]-*sn*-glycero-3-phosphocholine (NBD-PC; 3 mol %) (Avanti) was included in the lipid mix-

ture. Phospholipid concentrations were determined by a phosphate assay (Bartlett, 1959).

Light Scattering Measurements. Binding constants of BF1 and F-BF1 to small unilamellar vesicles were determined by light scattering (Nelsestuen & Lim, 1977). All solutions except lipid vesicles were passed through a 0.2-μm filter immediately before use. BF1 was preincubated with 10 mM $CaCl_2$ for 30 min (Marsh et al., 1979) before sequential additions to a magnetically stirred cuvette containing a 1.5-mL solution of 0.05 mg/mL lipid and 10 mM $CaCl_2$ or 1 mM Na_2EDTA in Tris buffer. Scattering intensities were corrected for sample volume increase and scatter due to unbound protein.

Instrumentation for Fluorescence Emission and Light Scattering. Tryptophan fluorescence (λ_{ex} = 280 nm; λ_{em} = 340 nm), fluorescein fluorescence (λ_{ex} = 494 nm; λ_{em} = 510–600 nm), and light scattering ($\lambda_{ex} = \lambda_{em}$ = 320 nm) were monitored with a spectrofluorometer (SLM 8000C, SLM Instruments, Inc., Urbana, IL).

Substrate-Supported Planar Membranes. Fused silica substrates (1" × 1" × 1 mm, Quartz Scientific Inc., Fairport Harbor, OH) and 3" × 1" glass microscope slides were cleaned with Linbro 7X detergent (Flow Laboratories) immediately before exposure to an argon ion plasma (PDC-3XG, Harrick Scientific Corp., Ossining, NY) for 15 min (Thompson et al., 1984). The fused quartz slides were mounted to glass slides by ~100-μm spacers. A 75-μL suspension of vesicles of defined PS content and lipid concentration was applied to the space between the slides and incubated at room temperature for 1–300 min. The volume between the slides was then rinsed with 3 mL of Tris buffer. For epifluorescence pattern photobleaching of NBD-PC in planar membranes, the quartz substrate with deposited lipid was removed under water and placed on a clean 3" × 1" glass microscope slide.

Langmuir–Blodgett Films. In some experiments, Langmuir–Blodgett monolayers composed of PS/POPC (30/70, mol/mol) were deposited at 35 dyne/cm on tetradecyltrichlorosilane-treated fused quartz surfaces, using previously described methods (Pisarchick & Thompson, 1990).

Sample Preparation. Planar membranes or Langmuir–Blodgett films were treated with 200 μL of 10 mg/mL BSA for 15 min, rinsed with 3 mL of Tris buffer, and then equilibrated with 250 μL of Tris buffer containing various concentrations of preincubated F-BF1 with 2 mg/mL BSA and 10 mM $CaCl_2$ or 1 mM Na_2EDTA. In some samples, the final solution applied to the planar membranes also contained glycerol (Fisher Scientific, Fair Lawn, NJ). The viscosities and therefore compositions of the glycerol solutions were confirmed using a Cannon L456 viscometer (Cannon Instrument Co., State College, PA). Refractive indices and concentrations of glycerol-containing solutions were obtained from the literature using measured viscosities (Weast, 1985).

Fluorescence Microscopy. The fluorescence microscope was composed of an argon ion laser (Innova 90-3, Coherent Inc., Palo Alto, CA), an inverted optical microscope (Zeiss IM-35, Eastern Microscope Co., Raleigh NC), and a single-photon-counting photomultiplier (31034A, RCA, Lancaster, PA) interfaced to an IBM PC AT computer (Wright et al., 1988).

Using substrate-supported planar membranes containing NBD-PC, membrane continuity was observed by TIRFM, and the lateral mobility of fluorescent lipids was examined by both fluorescence pattern photobleaching recovery (Smith & McConnell, 1978) and TIR/FPR (Burghardt & Axelrod, 1981). Conditions for pattern photobleaching were as described previously (Wright et al., 1988). Parameters for TIR-FPR were as described below.

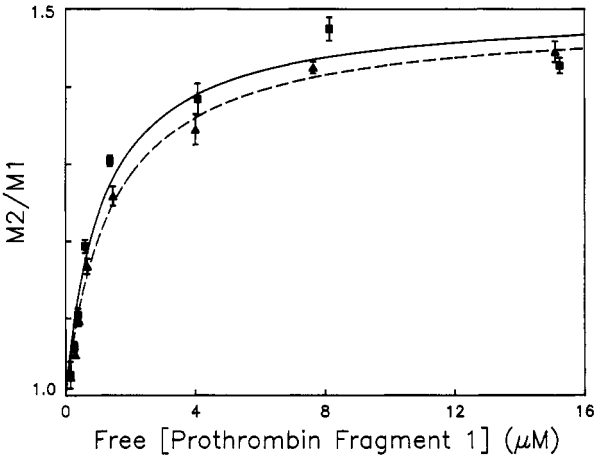

FIGURE 1: Binding of BF1 and F-BF1 to small unilamellar vesicles measured with light scattering. F-BF1 (▲) and BF1 (■) membrane binding was measured by plotting the ratio of the molecular weight of PS/POPC (25/75, mol/mol) vesicle–protein complexes (M_2) to the molecular weight of the vesicles (M_1) versus the free protein concentration. Data were corrected and analyzed according to Nelsestuen and Lim (1977). This procedure gave apparent equilibrium dissociation constants of 1.1 ± 0.1 μM for BF1 (—) and 1.5 ± 0.2 μM for F-BF1 (---). Solutions contained 0.05 mg/mL phospholipid and 10 mM Ca^{2+}. Each curve is an average of at least three independent trials; uncertainties are standard deviations of the means.

The fluorescence arising from membrane-bound F-BF1 was detected by TIRFM (Pisarchick & Thompson, 1990; Poglitsch & Thompson, 1990) with the following parameters: laser wavelength, 488 nm; laser power, 0.05–50 μW; fused silica prism, 1 cm^3; incidence angle θ, 75°; major and minor axes of the elliptically shaped evanescent illumination, 35 μm × 100 μm or 100 μm × 120 μm; objective (Nikon), air, 10×, 0.25 NA; focal length of auxiliary lens, 80 mm; evanescent wave depth, ~820 Å. TIR/FPR was carried out as described (Burghardt & Axelrod, 1981; Poglitsch et al., 1991) with the following additional parameters: bleaching beam power, 0.1–0.5 W; bleaching time, 10 ms–2 s; depth of bleach, 30–95%.

Data Analysis. BF1 binding curves constructed from light scattering data (Nelsestuen & Lim, 1977), fluorescence pattern photobleaching data (Wright et al., 1988), TIRFM binding curves (Pisarchick & Thompson, 1990), and TIR/FPR recovery curves (Thompson et al., 1981) were fit to theoretical functions using the ASYST iterative Gauss–Newton nonlinear curve fitting routine (Macmillan Software Co., New York).

RESULTS

Vesicle Binding Properties of F-BF1. Light scattering measurements demonstrated that conjugation with fluorescein did not significantly alter the apparent membrane association constant of BF1. Figure 1 shows light scattering data for both labeled and unlabeled BF1 binding to bovPS/POPC (25/75, mol/mol) small unilamellar vesicles with 10 mM Ca^{2+}. Quantitative analysis (Nelsestuen & Lim, 1977) of three to four independently obtained binding curves gave apparent membrane dissociation constants of K_d = 1.1 ± 0.1 μM for BF1 and K_d = 1.5 ± 0.2 μM for F-BF1. Thus, essentially no difference in binding constants was observed, suggesting that the presence of the probe on the protein did not significantly interfere with equilibrium membrane binding. In the absence of Ca^{2+}, protein binding to vesicles was not detected (data not shown).

Characterization of Planar Membranes. The deposition of lipid layers onto glass or fused silica substrates by the vesicle fusion procedure has been previously used for the formation

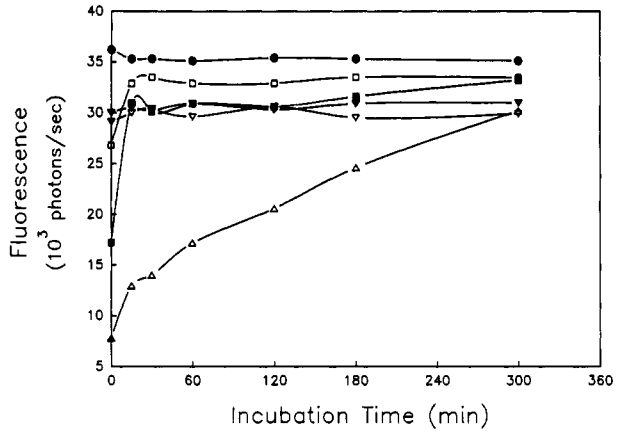

FIGURE 2: Small unilamellar vesicle fusion at quartz substrates. NBD-PC (3 mol %) incorporated into PS/POPC vesicles of various composition was used to examine vesicle deposition on quartz substrates. Evanescent excitation of adsorbed lipid was monitored by TIR/FPR for the following vesicle compositions: PC (●), PS/PC (5/95, mol/mol) (▽), PS/PC (15/85, mol/mol) (▼), PS/PC (25/75 mol/mol) (□), PS/PC (35/65, mol/mol) (■), PS/PC (50/50, mol/mol) (△). Vesicles were allowed to incubate with quartz surfaces for allotted times, and the surfaces were then rinsed with Tris buffer. Each data set is an average of at least two trials using independent vesicle preparations.

of continuous membranes on both planar surfaces (Brian & McConnell, 1984; Poglitsch & Thompson, 1990; Tendian et al., 1991; Zot et al., 1992) and capillary tubes (Gemmell et al., 1988; Schoen et al., 1990). In this work, substrate-supported planar membranes were constructed using a similar vesicle fusion-type procedure. Membranes were characterized using NBD-PC as a fluorescent probe for membrane continuity, stability, and lipid mobility.

Small unilamellar vesicles of varying phospholipid compositions (0–50 mol % PS; 97–47 mol % POPC; 3 mol % NBD-PC) were tested for their ability to form quartz-supported planar membranes. Using TIRFM, the fluorescence intensities of membranes were measured as a function of both the concentration of vesicle suspensions that were applied to substrates and the times for which substrates were treated with vesicle suspensions. For vesicles suspensions containing ≈2 mM phospholipid and less than 35 mol % PS, saturable lipid deposition occurred for incubation times ≥20 min; for 2 mM suspensions of vesicles composed of 50 mol % PS and 50 mol % PC, surface adsorption was much slower (Figure 2). For vesicles containing 25 mol % PS, surface saturation occurred after 20 min for phospholipid concentrations ≥0.5 mM (data not shown). Vesicle suspensions of ~2 mM phospholipid and incubation times of 30 min were used for all subsequent experiments.

Planar membranes formed from vesicles with 0–35 mol % PS showed approximately uniform fluorescence distributions within optical resolution, providing evidence for relatively continuous membranes. Lateral diffusion measurements, by fluorescence recovery after photobleaching of NBD-PC incorporated into membranes, showed that 75–90% of the fluorescent lipids had long-range lateral mobility with apparent diffusion coefficients in the range of $\sim 10^{-8}$ cm^2 s^{-1} (Table I). Previous studies using fluorescence techniques and ^{14}C-labeled phospholipids have shown that membranes constructed by similar methods form continuous, single phospholipid bilayers (Watts et al., 1984; Gemmell et al., 1988; Zot et al., 1992). Over a period of approximately 1 h, no significant change was observed in the fluorescence intensities of membranes. The addition of 10 mM Ca^{2+}, 1 mM EDTA, or glycerol did not significantly change the apparent NBD-PC lateral diffusion coefficient; however, equilibrating 25 mol % PS membranes with 25–41% glycerol solutions decreased the fractional mobility to ~60%. The mobility of NBD-PC incorporated into POPC membranes was slightly reduced with the addition of 5 mol % PS but was not further reduced for PS compositions up to 35 mol % PS.

Table I: Lateral Mobility of NBD-PC in Supported Planar Membranes[a]

supported planar membranes	sample	diffusion coefficient (10^{-8} cm^2 s^{-1})	fractional mobility
POPC/NBD-PC (97/3)	Tris buffer	1.39 ± 0.04	0.81 ± 0.05
PS/POPC/NBD-PC (5/92/3)	Tris buffer	0.93 ± 0.20	0.84 ± 0.06
PS/POPC/NBD-PC (15/82/3)	Tris buffer	1.04 ± 0.22	0.87 ± 0.03
PS/POPC/NBD-PC (25/72/3)	Tris buffer	1.08 ± 0.10	0.83 ± 0.03
PS/POPC/NBD-PC (35/62/3)	Tris buffer	1.00 ± 0.07	0.85 ± 0.04
PS/POPC/NBD-PC (25/72/3)	Tris buffer with 25–41% glycerol	1.02 ± 0.23	0.62 ± 0.02

[a] Lipid diffusion parameters are averages of between 5 and 10 TIR/FPR measurements from at least two independent vesicle preparations. Uncertainties are standard deviations of the means. Diffusion measurements obtained by epifluorescence pattern photobleaching agreed with those obtained by TIR spot photobleaching recovery. Membranes equilibrated with 10 mM Ca^{2+} or 1 mM EDTA in Tris buffer showed similar mobilities.

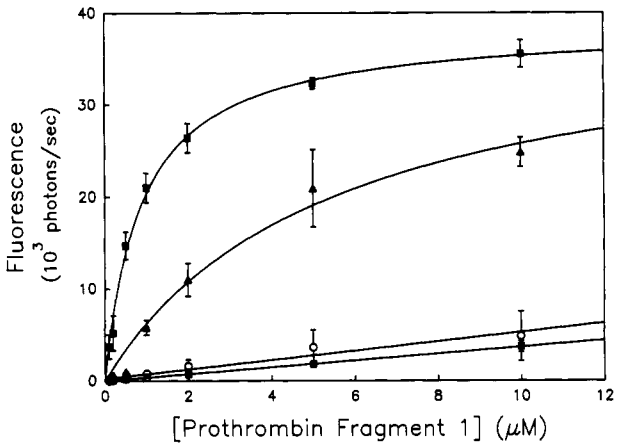

FIGURE 3: Binding of F-BF1 to planar membranes of various PS content. The evanescently excited fluorescence of F-BF1 on POPC planar membranes (○) and on 25 mol % PS planar membranes with 1 mM EDTA (□) was much lower than the fluorescence on PS-containing membranes with Ca^{2+}. The differences between the fluorescence intensities on 25 mol % PS membranes with 10 mM Ca^{2+} and on membranes with 1 mM EDTA (■) increased to apparent saturation with increasing F-BF1 solution concentrations. The fluorescence differences on 5 mol % PS membranes showed similar behavior (▲). Points are averages of at least five independent measurements from two to four vesicle and protein preparations, except that the 1 mM EDTA data set is the average of 10 trials from planar membranes of PS content between 0% and 35%. Uncertainties are shown as standard deviations of the mean. The differences of the F-BF1 fluorescence in the presence and absence of Ca^{2+} were fit to eq 11 to yield values of the apparent dissociation constant, K_d, and the maximum fluorescence, $F(\infty)$ (—).

Equilibrium Binding of Fragment 1 to Planar Membranes. The association of F-BF1 with PS/POPC planar membranes was examined by TIRFM (Figure 3). The evanescently excited fluorescence of F-BF1 on or near planar membranes was measured as a function of the solution concentration of F-BF1 in the presence of 1 mM EDTA or 10 mM Ca^{2+}. On membranes containing 5–35 mol % PS in the presence of Ca^{2+}, the fluorescence reached saturable levels, whereas the fluorescence of F-BF1 on POPC membranes and of F-BF1

Table II: Equilibrium Binding Characteristics of F-BF1 on Planar Membranes of Different PS Content[a]

planar membrane	K_d (μM)	$F(\infty)$ (10^3 photons s^{-1})
5/95 (mol/mol) PS/POPC	5.3 ± 0.1	39.6
15/85 (mol/mol) PS/POPC	3.8 ± 0.1	38.3
25/75 (mol/mol) PS/POPC	0.9 ± 0.2	38.5

[a] The best fit to the binding curve data, corrected for solution fluorescence by subtraction of the 1 mM EDTA control, was obtained using eq 11. This treatment yielded values for the dissociation constant, K_d, and the theoretical maximum fluorescence, $F(\infty)$. All non-control samples were prepared with 10 mM Ca^{2+}. Each measurement represents the average of two to four binding curves obtained from separate vesicle and protein preparations. Uncertainties are standard deviations of the means.

on PS/POPC membranes with EDTA was much lower in magnitude and increased linearly with the F-BF1 concentration. Thus, the binding of F-BF1 to the PS/POPC planar membranes was shown to be Ca^{2+}-dependent and to require the negatively charged phospholipids.

Several additional control measurements were carried out to further verify the Ca^{2+} and PS specificity of F-BF1 binding to PS/POPC planar membranes. First, on membranes containing 25 mol % PS, the fluorescence of 0.5 μM F-BF1 mixed with 4.5 μM BF1 and the fluorescence of 0.13 μM F-BF1 mixed with 4.87 μM BF1 was 10.5- and 36-fold lower, respectively, than the fluorescence of 5 μM F-BF1. These measurements demonstrated that excess unlabeled fragment 1 effectively competed with F-BF1 for membrane binding sites. Second, the fluorescence of 10 μM F-BF1 on quartz substrates that had not been treated with phospholipid vesicles was several-fold lower than the fluorescence of 10 μM F-BF1 on POPC planar membranes. This observation rules out the possibility that a significant fraction of the F-BF1 fluorescence on either PS/POPC or POPC planar membranes was associated with F-BF1 bound to "defect" regions of bare quartz. Third, the fluorescence arising from 3 μM F-BF1 on membranes with 25 mol % PS was reduced approximately 15-fold by washing with 1 mL of Tris buffer, demonstrating that the membrane binding was reversible. Fourth, neither the magnitude nor the shape of the emission spectra of fluorescein attached to BF1 were affected by either 10 mM Ca^{2+} or near saturation with 25 mol % PS phospholipid vesicles.

The data shown in Figure 3 imply an apparent membrane dissociation constant of $K_d \approx 1$ μM for F-BF1 on planar membranes containing 25 mol % PS (see below). Previous work has shown that the affinity of prothrombin and BF1 for PS/POPC membranes increases with PS content (Wei et al., 1982; Kop et al., 1984). Thus, planar membranes of varying PS content were constructed to investigate the equilibrium binding properties of F-BF1 on supported planar membranes as a function of surface charge. As shown in Figure 3 and Table II, the apparent dissociation constant increased with decreasing PS content; a 5-fold decrease in K_d was observed between 5% PS and 25% PS planar membranes. The trend of stronger binding to membranes with higher PS densities was not observed for planar membranes containing ≥35% PS. This observation suggests possible membrane irregularities and, for this reason, further investigation of the membrane-binding characteristics on planar membranes containing >25 mol % PS was not pursued. Also shown in Table II is the theoretical maximum fluorescence as determined by fitting the binding data to eq 11 (see below). Similar fluorescence maxima were obtained for membranes with PS content less than 25 mol %; however, the 35/65 PS/POPC membrane-binding isotherm yielded a higher value.

Surface Binding Kinetics of F-BF1 on PS/POPC Planar Membranes. Total internal reflection illumination coupled with fluorescence recovery after photobleaching (TIR/FPR) (Thompson et al., 1981; Burghardt & Axelrod, 1981) was used to investigate the kinetics of F-BF1 binding to acidic planar membranes. In this technique, the evanescently excited fluorescence associated with F-BF1 bound to or very close to the membrane surface is monitored before and after an intense pulse of the laser. Fluorescence recovery, detected as unbleached molecules replace surface-bound, bleached ones, is recorded as a function of time. In the time course of a typical TIR/FPR curve, control experiments in which samples were illuminated in the absence of a bleach pulse yielded a constant fluorescence signal.

Figure 4a shows a typical time-dependent TIR/FPR recovery curve for 5 μM F-BF1 on planar membranes containing 25 mol % PS. As shown, the recovery curves were not monoexponential. For an initial analysis, data were fit to the following theoretical form:

$$F(t) = F(-) - [a_0 + \sum_{i=1}^{n} a_i \exp(-k_i t)] \quad (1)$$

where a_i (for $i = 0$ to n) and k_i (for $i = 1$ to n) were free parameters. The fractional recovery associated with each rate was calculated as

$$r_i = \frac{a_i}{\sum_{i=0}^{n} a_i} \quad (2)$$

for $i = 0$ to n. In eq 2, r_0 is the fraction of bound, bleached F-BF1 that does not exchange with solution phase F-BF1 during the time range of fluorescence recovery.

TIR/FPR data were fit to eq 1 for one ($n = 1$), two ($n = 2$), and three ($n = 3$) reversible components. For all sample types on PS-containing membranes, analysis with an F statistic of the χ^2 goodness-of-fit parameter (Wright et al., 1988) indicated that the data were best described by two reversible components (i.e., two exponential terms). The values for the two rates, k_1 and k_2, and their associated fractional recoveries, r_1 and r_2, obtained from the best fits of TIR/FPR data to eq

Table III: TIR/FPR Reaction-Limited Dissociation Rates of F-BF1 on Planar Membranes (PS/POPC, 25/75)[a]

sample (TIR ellipse minor axis)	apparent dissociation rate k_1 (s^{-1})	apparent dissociation rate k_2 (s^{-1})	fractional recovery r_1	fractional recovery r_2	k^a_{off} (s^{-1})
5 μM F-BF1 (~35 μm)	0.23 ± 0.01	0.025 ± 0.002	0.40 ± 0.02	0.28 ± 0.01	0.097 ± 0.006
10 μM F-BF1 (~35 μm)	0.28 ± 0.04	0.018 ± 0.002	0.43 ± 0.01	0.25 ± 0.01	0.12 ± 0.01
20 μM F-BF1 (~35 μm)	0.32 ± 0.02	0.016 ± 0.001	0.37 ± 0.01	0.25 ± 0.01	0.13 ± 0.01
5 μM F-BF1 (~100 μm)	0.26 ± 0.01	0.030 ± 0.002	0.35 ± 0.02	0.29 ± 0.01	0.100 ± 0.001
Langmuir–Blodgett monolayer, 20 μM F-BF1 (~35 μm)	0.26 ± 0.05	0.020 ± 0.003	0.30 ± 0.02	0.300 ± 0.003	0.08 ± 0.02

[a] Values of k^a_{off} measured by TIR/FPR are averages of 15–20 measurements from at least three F-BF1 and vesicle preparations. Errors are shown as standard deviations of the means. Analysis of the nonmonoexponential fluorescence recovery curves was carried out by fitting to eq 1 with $n = 2$. F statistics showed this analysis to be appropriate. All samples contained 10 mM Ca^{2+} and 25/75 PS/POPC planar membranes with the exception that Langmuir–Blodgett monolayers were 30/70 PS/POPC.

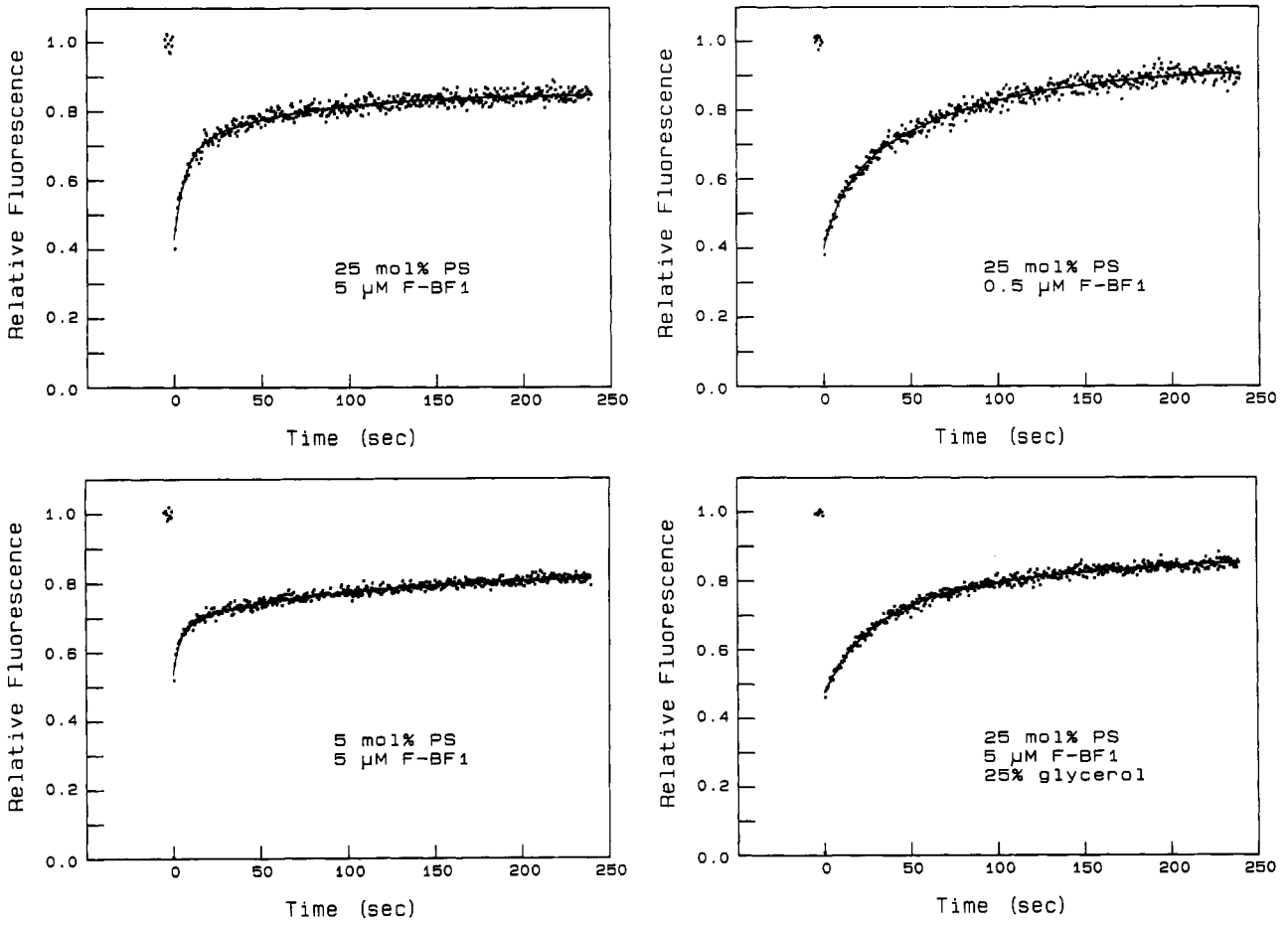

FIGURE 4: Representative TIR/FPR fluorescence recovery curves. All curves were obtained for F-BF1 in the presence of 10 mM Ca^{2+}. Typical recovery curves are shown for (a, top left) 5 μM and (b, top right) 0.5 μM F-BF1 on a 25/75 (mol/mol) PS/POPC planar membrane, (d, bottom right) 5 μM F-BF1 on a 25/75 (mol/mol) PS/POPC planar membrane containing 25% glycerol, and (c, bottom left) 5 μM BF1 on a 5/95 (mol/mol) PS/POPC membrane. The lines show the best fits to eq 1 with $n = 2$.

Table IV: TIR/FPR Transport-Limited Dissociation Rates of F-BF1 on Planar Membranes (PS/POPC, 25/75)[a]

sample	apparent dissociation rate		fractional recovery		
	k_1 (s^{-1})	k_2 (s^{-1})	r_1	r_2	k^a_{off} (s^{-1})
0.2 μM BF1	0.039 ± 0.005	0.006 ± 0.001	0.22 ± 0.01	0.67 ± 0.13	0.011 ± 0.002
0.5 μM BF1	0.08 ± 0.01	0.012 ± 0.001	0.21 ± 0.03	0.62 ± 0.03	0.024 ± 0.004
1.0 μM BF1	0.16 ± 0.02	0.022 ± 0.003	0.21 ± 0.03	0.50 ± 0.03	0.045 ± 0.005
2.0 μM BF1	0.17 ± 0.05	0.023 ± 0.006	0.41 ± 0.03	0.40 ± 0.01	0.08 ± 0.01
5 μM BF1, 25% glycerol	0.059 ± 0.005	0.013 ± 0.001	0.31 ± 0.04	0.41 ± 0.03	0.022 ± 0.001
5 μM BF1, 41% glycerol	0.05 ± 0.02	0.009 ± 0.002	0.19 ± 0.04	0.48 ± 0.01	0.012 ± 0.002
10 μM BF1, 38% glycerol	0.07 ± 0.02	0.006 ± 0.002	0.16 ± 0.06	0.55 ± 0.07	0.012 ± 0.003

[a] Values are averages of between five and eight measurements. Values for 0.5, 1.0, and 2.0 μM F-BF1 were obtained from at least three independent lipid vesicle and protein preparations. All samples contained 10 mM Ca^{2+}. Analysis of the nonmonoexponential fluorescence recovery curves was carried out by fitting to eq 1 with $n = 2$. F statistics showed this analysis to be appropriate. Uncertainties are standard deviations of the means.

1 are shown in Table III for different sample types. Also given are the average recovery rates k^a_{off}, calculated as

$$k^a_{off} = r_1 k_1 + r_2 k_2 \quad (3)$$

The mean F statistics for comparing the best fits to eq 1 with $n = 1$ or 2, and with $n = 2$ or 3, were determined as described by Wright et al. (1988). A statistically better fit yields a value of $F > 3$. For all recovery curves of F-BF1 on PS/POPC planar membranes, a clearly better fit was obtained with $n = 2$ (with five free parameters) over $n = 1$ (with three free parameters) ($F \approx 99$). Comparison of most curves fit with $n = 2$ and $n = 3$ yielded an average F statistic significantly lower ($F \approx 4$). For BF1 on POPC membranes, comparison of fits to eq 1 with $n = 2$ and $n = 1$ yielded an F statistic of $F \approx 5$.

For TIR/FPR with a very large illumination area, diffusion rates parallel to the surface are in theory negligibly small and do not contribute to the fluorescence recovery (Thompson et al., 1981). Support for this condition was obtained by observing fluorescence recovery rates as a function of the size of the illuminated area. Increasing the width of the spot 3-fold did not produce a significant change in either the fluorescence recovery rates or the fractional recoveries (Table III).

Effect of F-BF1 Solution Concentration on Surface Binding Kinetics. Figure 4b shows a typical TIR/FPR recovery curve for 0.5 μM F-BF1 on 25 mol % PS planar membranes. As shown, the fluorescence recovery was significantly slower than that measured for 5 μM F-BF1 on membranes of the same composition. At low solution concentrations, the recovery rate was strongly dependent on the F-BF1 solution concentration (Table IV), and, at high solution concentrations, the rate was approximately independent of the solution concentration (Table III). These results suggest that the rate of fluorescence recovery is limited by the rate of solution transport at low F-BF1

Table V: Fluorescence Recovery Rates Measured by TIR/FPR of F-BF1 on Planar Membranes of Various PS Content[a]

planar membrane	sample (μM BF1)	apparent dissociation rate k_1 (s^{-1})	apparent dissociation rate k_2 (s^{-1})	fractional recovery r_1	fractional recovery r_2	average k^a_{off} (s^{-1})	average k^a_{on} (M^{-1} s^{-1}) × 10^{-5}
0/100 (mol/mol) PS/POPC	10	0.026 ± 0.004		0.45 ± 0.04			
5/95 (mol/mol) PS/POPC	10	0.29 ± 0.04	0.012 ± 0.001	0.24 ± 0.01	0.40 ± 0.02	0.07 ± 0.01	0.13 ± 0.02
	20	0.28 ± 0.03	0.012 ± 0.002	0.21 ± 0.01	0.47 ± 0.02	0.063 ● 0.007	0.12 ± 0.12
15/85 (mol/mol) PS/POPC	10	0.38 ± 0.04	0.015 ± 0.001	0.35 ± 0.01	0.29 ± 0.01	0.13 ± 0.01	0.34 ● 0.04
	20	0.37 ± 0.03	0.015 ± 0.001	0.32 ± 0.01	0.32 ± 0.01	0.13 ± 0.01	0.34 ± 0.03
25/75 (mol/mol) PS/POPC	10	0.28 ± 0.04	0.018 ± 0.002	0.43 ± 0.01	0.25 ± 0.01	0.12 ± 0.01	1.33 ± 0.11
	20	0.32 ± 0.02	0.016 ± 0.001	0.37 ± 0.01	0.25 ± 0.01	0.13 ± 0.01	1.44 ± 0.11

[a] The values are averages of between 16 and 22 measurements using at least three independent protein and lipid vesicle preparations. k^a_{on} was determined by $k^a_{on} = k^a_{off}/K_d$. Dissociation rates and averages were determined by the analysis described in the text. Analysis of the nonmonoexponential fluorescence recovery curves was carried out by fitting to eq 1 with $n = 2$. F statistics showed this analysis to be appropriate. Uncertainties are standard deviations of the means. All measurements were conducted in the presence of 10 mM Ca^{2+}.

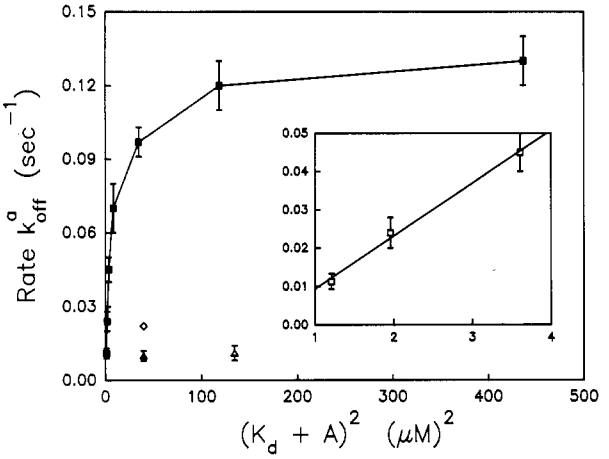

FIGURE 5: Dependence of fluorescence recovery rate on F-BF1 solution concentration. Fluorescence recovery rates k_1 and k_2 and fractional recoveries r_1 and r_2 were determined from the best fits of TIR/FPR data to eq 1 with $n = 2$ and used to calculate the average rate k^a_{off} according to eq 3. Rates are plotted versus $(K_d + A)^2$ according to eq 16. Linear regression of the data at low F-BF1 concentrations yields a slope of 0.014 μM^{-2} s^{-1} (inset), which is approximately equal to $D/N^2 = 0.027$ μM^{-2} s^{-1}. Samples contained 10 mM Ca^{2+} and 25 mol % PS. Also shown are the recovery rates obtained from samples containing glycerol: 5 μM BF1, 25% glycerol (◇); 5 μM BF1, 41% glycerol (▲); 10 μM BF1, 38% glycerol (△).

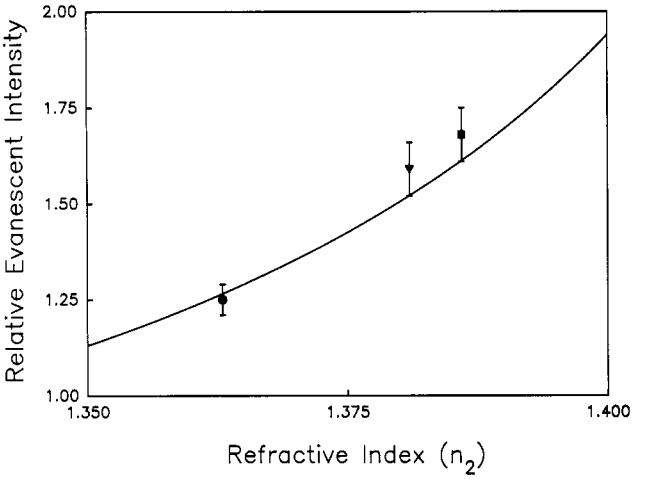

FIGURE 6: Effect of solution refractive index on evanescent intensity. The relative fluorescence of NBD-PC in 25/75 (mol/mol) PS/POPC membranes, as measured by TIRFM, increased with the solution refractive index according to eq 6 (—). Shown are samples containing 41% (■), 38% (▼), and 25% (●) glycerol. Points are averages and standard deviations of the means for 20 measurements from three separate samples.

solution concentrations but is limited by the intrinsic rate(s) of surface association/dissociation at higher F-BF1 solution concentrations. Figure 5 shows the concentration dependence of the average rate of fluorescence recovery, k^a_{off}, as a function of the solution concentration of F-BF1, for planar membranes containing 25 mol % PS.

Kinetics of F-BF1 Binding in Glycerol Solutions. To provide additional evidence that TIR/FPR recovery curves were transport-limited at low F-BF1 solution concentrations but reaction-limited at high F-BF1 solution concentrations, data were obtained for samples in which the solution viscosity was increased using glycerol. Membrane continuity and lipid lateral diffusion (Table I) were found to be relatively unaffected by glycerol-containing solutions. For 5 and 10 μM F-BF1 on membranes containing 25 mol % PS, the rates of TIR/FPR fluorescence recovery were significantly slowed by high concentrations of glycerol (Figure 4 and Table IV). As discussed below, the solution refractive index was significantly changed by the glycerol, which caused significant NBD-PC intensity changes, as predicted by the theory for total internal reflection (Figure 6).

Effect of Membrane Composition on the Binding Kinetics of F-BF1. TIR/FPR recovery curves were obtained on planar membranes containing <25 mol % PS to investigate the effect of acidic lipid content on association/dissociation kinetic rates. Data were obtained for F-BF1 solution concentrations ≥5 μM, where it was expected that fluorescence recovery would not depend on the F-BF1 solution concentration. Recovery curves were fit to eq 1 to obtain best-fit values for the rates, k_1 and k_2, and their fractional recoveries, r_1 and r_2, as described above (Table V). There was no statistically significant difference in the fitting parameters for membranes treated with 10 or 20 μM BF1. This result is consistent with the data for membranes containing 25 mol % PS and supports the claim that the fluorescence recovery is largely reaction-limited at high F-BF1 concentrations. As the PS density in the planar membranes was increased from 5 to 25 mol %, the average dissociation rate k^a_{off} increased approximately 2-fold. This effect was due mostly to the distribution of the percent recovery from the two rates; i.e., at 5 mol % PS, fluorescence recovery was dominated by the slower dissociation rate, and at 25 mol % PS, recovery was dominated by the faster rate (Table V and Figure 4). Increasing the PS content of the membranes from 5 to 25 mol % resulted in a 10-fold increase of apparent association rate, calculated as $k^a_{on} = k^a_{off}/K_d$. This trend has been previously observed for prothrombin on vesicles (Wei et al., 1982).

TIR/FPR Recovery Curves on Other Surfaces. Although the steady-state fluorescence was low for F-BF1 on membranes composed of 100 mol % POPC (Figure 3), the fluorescence was high enough to carry out TIR/FPR measurements. These data showed that, for 10 μM F-BF1, ≈50% of the bleached

fluorescence recovered with a characteristic time of ≈50 s.

To test the validity of the kinetic data obtained using vesicle fusion-type planar membranes, a set of TIR/FPR recovery curves for 20 μM F-BF1 on Langmuir–Blodgett monolayers composed of 30 mol % PS and 70 mol % POPC was obtained (Table III). These data gave values of the best-fit parameters that were approximately equivalent to those on vesicle fusion-type membranes.

TIR/FPR Bleachabilities. The fraction of the evanescently excited fluorescence that arose from bound F-BF1 rather than from F-BF1 that was in solution but close enough to the surface to be excited by the evanescent field was determined by measuring the fraction of the fluorescence that was bleachable (Schmidt et al., 1990). For 10 μM F-BF1 on membranes containing 25 mol % PS, greater than 95% of the evanescently excited fluorescence was bleachable. For 10 μM F-BF1 on POPC membranes, ≥50–70% of the fluorescence could be bleached and was therefore associated with surface-bound F-BF1. This result is consistent with previous work suggesting that prothrombin fragment 1 binds weakly to POPC membranes (Tendian et al., 1991). For 10 μM F-BF1 on quartz surfaces that had not been treated with phospholipid vesicles, the fluorescence was very low and not effectively bleached.

The result that F-BF1 on PS/POPC planar membranes was approximately 100% bleachable provides evidence that a recovery component much faster than those observed does not exist. If rapid binding and dissociation were present, a fraction of the prebleach fluorescence would not be bleachable. Furthermore, if binding and dissociation that was only slightly faster than the measured TIR/FPR data was present, the rates of fluorescence recovery would depend on the bleaching duration. However, TIR/FPR recovery curves did not measurably change with bleaching times ranging from 10 ms to 2 s.

Irreversible Fractions. As shown in Table III, the total fractional fluorescence recovery for F-BF1 on PS/POPC membranes, $r_1 + r_2$, was ≈70%, strongly suggesting that 30% of the F-BF1 bound to the PS/POPC planar membranes with a dissociation rate slower than the time scale of the measurements (several minutes). In general, another possibility is that some of the "irreversibly" bound F-BF1 was associated with areas not covered with membrane (i.e., "defect" regions of bare quartz). However, even though inclusion of BSA in solution resulted in slight improvements of fractional recoveries while not influencing recovery rates, control experiments (see above) showed that F-BF1 bound to bare quartz only with very low affinity. A third possibility is that the irreversible adsorption was induced by the photobleaching pulse (perhaps by photoinduced covalent surface chemistry). This explanation is unlikely because the irreversible fraction did not change with significant increases in the length of the bleach pulse (200-fold) or with increases in the bleaching intensity (5-fold).

Other Control Measurements. Several experiments were carried out to investigate the possibility that the biphasic nature of recovery was due to an experimental artifact. The formation of photoinduced cross-linking products, such as dimers, as result of a laser pulse has been observed in some previous works (Sheetz & Koppel, 1979). However, no change in either of the rates of fluorescence recovery or in the fractional recoveries was observed when the bleach pulse length was increased through a range of 10 ms–2 s; thus, photodamage effects are unlikely. The possibility that the inclusion of BSA in the sample to reduce nonspecific adsorption to the quartz caused irregular binding behavior was also eliminated. TIR/FPR on F-BF1 samples with and without BSA yielded the same rates of recovery, implying that BSA effectively blocked irreversible, nonspecific adsorption without influencing the membrane-binding properties of F-BF1.

Quantitative Analysis of Binding and Kinetic Data

Evanescently Excited Fluorescence. In steady-state TIRFM measurements, an argon ion laser beam is incident at the interface of the planar quartz surface, which supports a model membrane, and an adjacent buffered aqueous solution containing F-BF1. Adsorbed F-BF1 is excited by the evanescent field, which decays in intensity as an exponential function of the distance from the interface, i.e.,

$$I(z) = I(0) \exp(-z/d) \tag{4}$$

where $I(z)$ is the evanescent intensity, z is the distance from the model membrane,

$$d = \frac{\lambda_0}{4\pi\sqrt{n_1^2 \sin^2 \theta - n_2^2}} \tag{5}$$

$\lambda_0 \approx 488$ nm is the vacuum wavelength, $\theta \approx 75°$ is the angle of incidence, $n_1 \approx 1.47$ is the refractive index of the quartz, and $n_2 \approx 1.33$ is the refractive index of the F-BF1 solution. These optical parameters give $d \approx 820$ Å. Equations 4 and 5 hold only when the planar membrane is much thinner than the evanescent wave depth. Previous studies have provided evidence that planar membranes formed by vesicle fusion methods are single phospholipid bilayers (Brian et al., 1984; Gemmell et al., 1988; Zot et al., 1992).

The characteristics of evanescent fields created at interfaces are in theory dependent on the refractive indices of the two media that form the interface (Axelrod et al., 1984). In particular, for a given incident intensity, incidence angle Θ, and higher refractive index n_1, both the evanescent intensity at the interface and the evanescent field depth increase with the lower refractive index. Specifically, for the *s*-polarized case in this work,

$$\frac{I(0)}{I(0)^\circ} = \left[\frac{1 - (n_2^\circ/n_1)^2}{1 - (n_2/n_1)^2}\right] \tag{6}$$

where $I(0)$ and $I(0)^\circ$ are the evanescent intensities at the interface for lower refractive indices equal to n_2 and n_2°. Equation 6 is illustrated in Figure 6 along with the measured relative fluorescence intensities of NBD-PC in planar membranes. The solution refractive index n_2 was varied by increasing the glycerol content (see Materials and Methods). These data support the validity of eq 6.

Because the angular emission profile for fluorescence and therefore the fluorescence collection efficiency is strongly affected by nearby dielectric interfaces (Reichert et al., 1987), the measured fluorescence is not necessarily proportional to the excitation intensity (eq 4). However, in this work, the fluorescence is collected from the low refractive index half-space and with a microscope objective (see Materials and Methods), and the anisotropic effects on fluorescence collection are small (Burghardt & Thompson, 1984). Assuming these effects to be negligible, the measured fluorescence is given by

$$F = QI(0)\left[C + A\int_0^\infty \exp(-z/d)\, dz\right] = QI(0)(C + Ad) \tag{7}$$

where Q is a proportionality constant, C is the two-dimensional density of bound F-BF1, and A is the three-dimensional solution concentration of F-BF1. In some samples, e.g., F-BF1

on PS/POPC membranes in the presence of Ca^{2+}, most of the excited fluorescence arises from surface-bound F-BF1, $C \gg Ad$, $F \approx QI(0)C$, and the fluorescence is approximately proportional to the surface density of bound molecules. In other samples, e.g., F-BF1 on untreated quartz, the fluorescence arises primarily from F-BF1 molecules that are in solution and near to the surface but not bound, $Ad \gg C$, $F \approx QI(0)Ad$, and the fluorescence is approximately proportional to the solution concentration of F-BF1.

Quantitative Estimates of Binding Site Densities. The surface density of F-BF1 bound to PS/POPC planar membranes in the presence of Ca^{2+} is proportional to $B(+)F(+)$, where $F(+)$ is the steady-state fluorescence and $B(+)$ denotes the bleachable fraction; and the density Ad is proportional to $[1 - B(-)]F(-)$, where $F(-)$ is the steady-state fluorescence from samples in the absence of Ca^{2+} and $B(-)$ is the bleachable fraction in the absence of Ca^{2+}. Thus, the ratio C/Ad may be estimated from the measured parameters $F(+)$, $F(-)$, $B(+)$, and $B(-)$ by

$$\frac{C}{Ad} = \frac{B(+)F(+)}{[1 - B(-)]F(-)} \tag{8}$$

For 25 mol % PS membranes and 10 μM F-BF1, $F(+)/F(-) \approx 22$, $B(+) \approx 0.95$, and $B(-) \geq 0.6$; thus, $C/Ad \geq 52$ and, using the known values of A and d, $C \geq 26\,000$ molecules/μm^2 (or ≤ 3800 Å^2/molecule). Because the membranes are saturated for 10 μM F-BF1, this density is an estimate of the *total* surface density of F-BF1 binding sites, denoted here by N.

Equilibrium Binding Curves for Simple Bimolecular Reactions Occurring at a Surface. When the measured fluorescence is proportional to the density of bound F-BF1, apparent surface association constants may be measured by recording the evanescently excited fluorescence as a function of the solution concentration of fluorescent ligands (Pisarchick & Thompson, 1990; Poglitsch et al., 1991). The simplest surface reaction may be modeled as occurring between monovalent ligands in solution and monovalent surface sites. In this model,

$$A + B \underset{k_{off}}{\overset{k_{on}}{\rightleftharpoons}} C$$

where A and C are defined above and B is the two-dimensional density of free (unoccupied) surface binding sites, k_{on} and k_{off} are the association and dissociation kinetic rates, respectively, and

$$K_d = \frac{k_{off}}{k_{on}} = \frac{AB}{C} \tag{9}$$

is the equilibrium dissociation constant. The total density of surface binding sites, N, is related to the surface densities of unoccupied, B, and occupied, C, sites as

$$N = B + C \tag{10}$$

Assuming that the surface-associated fluorescence is proportional to the density of bound F-BF1, then eqs 7 (with $Ad \approx 0$), 9, and 10 imply that the fluorescence as a function of the F-BF1 solution concentration, A, is given by

$$F(A) = \frac{F(\infty)A}{K_d + A} \tag{11}$$

where $F(\infty) = QI(0)N$.

To analyze the binding data for this simple binding mechanism, the fluorescence intensities for F-BF1 on PS/POPC membranes in the presence of EDTA were subtracted from the fluorescence intensities of F-BF1 on PS/POPC membranes in the presence 10 mM Ca^{2+}. The best fits of the fluorescence differences (which are approximately proportional to C) to eq 11 were determined by nonlinear regression with K_d and $F(\infty)$ as free parameters (Table II). For F-BF1 on 25 mol % PS membranes, this analysis gave $K_d = 0.9 \pm 0.2$ μM, which is comparable to that obtained by light scattering and other methods (Mann et al., 1990).

TIR/FPR Recovery Curves for Simple Bimolecular Surface Reactions. The measured TIR/FPR recovery curves were nonmonoexponential for all solution concentrations of F-BF1, for membrane compositions ranging from 5 to 35 mol % PS, and in the presence of glycerol (Figure 4 and Tables III, IV, and V). In this section, the ability of the simple binding mechanism shown above (in which monovalent F-BF1 reversibly binds to monovalent surface sites) to explain this property of the measured TIR/FPR data is addressed.

Previous theoretical work (Thompson et al., 1981) has shown that, for this binding mechanism, the shape of TIR/FPR recovery curves is a rather complex function that depends on the intrinsic dissociation rate, k_{off}, and three transport rates:

$$R_N = \frac{D_{soln}}{h^2} \tag{12}$$

$$R_L = \frac{D_{soln}}{s^2} \tag{13}$$

$$R_s = \frac{D_{surf}}{s^2} \tag{14}$$

In eqs 12–14, D_{soln} is the diffusion coefficient of F-BF1 in solution, D_{surf} is the diffusion coefficient of membrane-bound F-BF1, s is the semiminor axis of the illuminated area and

$$h = \frac{C}{A} \tag{15}$$

The rate k_{off} is the intrinsic dissociation rate and is a priori unknown. R_N (eq 12) is the rate of transport in solution through h, which gives the thickness of a slab next to the surface that contains a two-dimensional density of unbleached molecules sufficient to replace the density of surface-bound, bleached molecules. Equations 9, 10, 12, and 15 imply that

$$R_N = \frac{D_{soln}(K_d + A)^2}{N^2} \tag{16}$$

Figure 7 shows predicted values for R_N, calculated from eq 16 using values for N that are approximately 2-fold lower and 2-fold higher than the values estimated from eq 8. For $K_d = 0.9$ μM (25 mol % PS), $D_{soln} = 5 \times 10^{-7}$ cm^2 s^{-1} and $A = 0.5$–20 μM, R_N is expected to range from 0.21 to 46.8 s^{-1} (for $N \approx 13\,000$ molecules/μm^2) and 0.01–2.9 s^{-1} (for $N \approx 52\,000$ molecules/μm^2).

R_L (eq 13) and R_s (eq 14) are the rates of transport in solution and on the surface, respectively, through the illuminated surface area. These rates are larger and more prominent for optical geometries that use more focused beams (and have smaller values of s). In this work, the semiminor radius of the illuminated area is ≈ 18 μm and the solution diffusion coefficient of F-BF1 is $D_{soln} \approx 5 \times 10^{-7}$ cm^2 s^{-1}, which imply that $R_L \approx 0.15$ s^{-1}. In addition, the maximum surface diffusion coefficient of bound F-BF1 may be estimated as the lipid diffusion coefficient ($D_{surf} \leq 10^{-8}$ cm^2 s^{-1}; Table I), which gives $R_s \leq 0.003$ s^{-1}.

Recoveries due to surface diffusion (R_s) and surface association/dissociation (k_{off}, R_N, R_L) act approximately in parallel; i.e., the faster of these two processes dominates the rate of fluorescence recovery. Thus, because the estimated value of R_s is much less than the observed rate of fluorescence

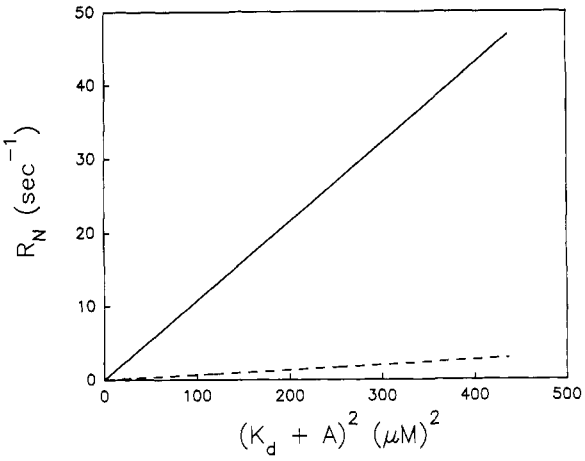

FIGURE 7: Theoretical values of R_N. The theoretical change in R_N as a function of F-BF1 solution concentration was calculated from eq 16. Curves were generated for 25 mol % PS using a surface site density 2-fold higher (52 000 molecules/μm^2) (---) and 2-fold lower (13 000 molecules/μm^2) (—) than the value estimated from equilibrium binding data. Other parameters were $K_d = 0.9$ μM and $D_{soln} = 5 \times 10^{-7}$ cm^2 s^{-1}.

recovery, surface diffusion is not expected to affect the TIR/FPR data. This expectation was confirmed by the experimental result that the recovery curves did not measurably change when the illuminated area was increased by a factor of ~10 (Table III).

In the absence of surface diffusion effects, surface dissociation (k_{off}) and solution transport (R_N and R_L) act approximately in series; i.e., the slower of the two processes dominates the rate of fluorescence recovery. Thus, because R_L is approximately equal to the fluorescence recovery rate (see above), the process associated with this rate (diffusion in the bulk solution parallel to the membrane) might be responsible for, and limit, the rate of fluorescence recovery. However, R_L depends sharply on the size of the illuminated area and, for high F-BF1 solution concentrations, the TIR/FPR data do not change with an increase in this area (Table III). This apparent inconsistency can be explained by noting that the rate of replenishment of surface-bound, bleached molecules will be determined by the larger of R_N and R_L and that $R_N \gg R_L$ for the F-BF1 solution concentration at which the dependence of the TIR/FPR recovery curves on the size of the illuminated area was examined. Thus, it can be concluded that, for a large illuminated area with reaction-limited sample conditions (high F-BF1 solution concentrations), the transport process associated with R_L does not significantly affect the observed recovery curves. A change in the TIR spot size might influence the fluorescence recovery rate at low F-BF1 solution concentrations by changing the relative magnitudes of R_N and R_L.

In the limit of a large illuminated area, the fluorescence recovery curve $F(t)$ depends only on the intrinsic dissociation rate k_{off} and the transport rate R_N (Thompson et al., 1981). Furthermore, when s approaches ∞

$$F(t) = F(\infty) + [F(0) - F(\infty)]G(t) \quad (17)$$

where

$$G(t) = \frac{1}{b_2 - b_1}[b_2 w(-ib_1\sqrt{k_{off}t}) - b_1 w(-ib_2\sqrt{k_{off}t})] \quad (18)$$

$$w(iz) = \exp(z^2)\,\mathrm{erfc}(z) \quad (19)$$

$$2b_{1,2} = \sqrt{\frac{k_{off}}{R_N}}\left[-1 \pm \sqrt{1 - \frac{4R_N}{k_{off}}}\right] \quad (20)$$

In eqs 17–20, $G(t)$ ranges from 1 (at $t = 0$) to 0 (as t approaches ∞) and gives the shape of the recovery.

There are two more simple limits in the case of a large illuminated area. If $k_{off} \ll R_N$, then the rate of solution transport is much faster than the intrinsic dissociation rate and surface-bound bleached molecules are replaced by unbleached molecules in solution immediately after they dissociate. In this situation, $G(t)$ is limited solely by the intrinsic rate of surface dissociation, $b_1 \approx i$ and $b_2 \approx -i$, and eqs 18–20 reduce to

$$G(t) = \exp(-k_{off}t) \quad (21)$$

In this "reaction limit", fluorescence recovery curves are monoexponential and do not depend on the solution concentration of F-BF1. On the other hand, if $R_N \ll k_{off}$, then the rate of solution transport is much slower than the intrinsic dissociation rate, bleached molecules are replaced by unbleached molecules only after diffusion through the distance h, and eqs 18–20 reduce to

$$G(t) = w(i\sqrt{R_N t}) \quad (22)$$

In the "diffusion limit", the fluorescence recovery curves are not monoexponential. Also, the rate of fluorescence recovery depends strongly on the solution concentration of F-BF1 and is proportional to $(K_d + A)^2$ (see eq 16).

If the nonmonoexponential shape of the TIR/FPR recovery curves was due to the nonexponential shape of eq 18 (or eq 22), the measured average recovery rate, k^a_{off}, would increase with the solution concentration of F-BF1. As shown in Figure 5, the rate depended on the F-BF1 concentration at low concentrations but was independent of the F-BF1 solution concentration at high concentrations. At very low solution concentrations, k^a_{off} was linear with $(K_d + A)^2$. Ignoring contributions from R_L, the slope for these transport-limited recovery curves should be D/N^2 (eq 16). Using $D = 5 \times 10^{-7}$ cm^2 s^{-1} and $N \geq 26\,000$ molecule/μm^2, D/N^2 is predicted to be ≤ 0.027 μM^{-2} s^{-1}; linear regression of the transport-limited data points in Figure 5 yielded a slope of 0.014 μM^{-2} s^{-1}, which compares favorably to the theoretically predicted value. Comparison of Figures 5 and 7 shows that, for F-BF1 solution concentrations between 0.5 and 5 μM, the measured fluorescence recovery rates are somewhat slower than the predicted R_N values. Therefore, the nonmonoexponential behavior of the TIR/FPR recovery curves at low F-BF1 solution concentrations might arise at least in part from a coupling between the rates of solution transport and intrinsic surface reaction.

For F-BF1 solution concentrations above 5 μM, the fluorescence recovery rate was not concentration dependent. This result suggests that the fluorescence recovery curves were primarily reaction-limited and that the nonmonoexponential behavior was not to due a coupling of the intrinsic surface binding kinetics and solution transport. To further support this conclusion, fluorescence recovery curves were simulated using eqs 18–20 for various ratios of $R_N/k_{off} > 1$ and then fit to a biexponential shape (eq 1 with $F(-) = 1$, $r_i = a_i$, $r_0 = 0$, and $r_1 = 1 - r_2$) with the time axis ranging from 0 to $10/k_{off}$. For 10 and 20 μM F-BF1, the values of R_N/k^a_{off} are equal to 27 and 91, respectively (see above). The simulated curves for these ratios were approximately equal to a biexponential shape with $k_1 = k_{off}$, $k_2 = 0.13\ k_{off}$, and $r_1 = 1 - r_2 = 0.87$ ($R_N/k_{off} = 27$) or $r_1 = 1 - r_2 = 0.92$ ($R_N/k_{off} = 91$). These results show that the fractional recovery from the slow component is much less, and that the fractional recovery from the fast component is much greater, than those from biexponential analysis of experimental curves (Table III). Also, Table III shows that

Table VI: Calculated Membrane Binding Parameters Using the Model for Multiple Conformations of Bound F-BF1[a]

planar membrane	$k_{off}(1)$ (s^{-1})	$k_{on}(1)$ (μM^{-1} s^{-1})	$K_d(1)$ (μM)	$k_{off}(2)$ (s^{-1})	$k_{on}(2)$ (s^{-1})	$K_d(2)$
5/95 (mol/mol) PS/POPC	0.25 ± 0.02	0.019 ± 0.002	14.5 ± 0.6	0.014 ± 0.001	0.022 ± 0.002	0.62 ± 0.03
15/85 (mol/mol) PS/POPC	0.35 ± 0.03	0.052 ± 0.005	7.0 ± 0.2	0.015 ± 0.001	0.014 ± 0.002	1.4 ± 0.2
25/75 (mol/mol) PS/POPC	0.32 ± 0.02	0.23 ± 0.02	1.4 ± 0.3	0.017 ± 0.001	0.009 ± 0.002	1.9 ± 0.2

[a] Kinetic and equilibrium parameters were calculated using the analysis described in the text. These determinations were made using the 20 μM F-BF1 data from Table V. Uncertainties are standard deviations of the means.

neither r_1 nor r_2 are affected by an increase in the F-BF1 solution concentration from 10 to 20 μM. Therefore, the nonmonoexponential character of the fluorescence recovery curves at high F-BF1 solution concentrations cannot be explained as a transport effect, and the fluorescence recovery shapes for these samples are not well described by the theoretical form for a simple reversible bimolecular reaction (eq 21). For these "reaction-limited" data, more complex surface binding mechanisms are considered.

Multiple Binding Site Types. One possibility is that the PS/POPC membrane surfaces contain more than one type of binding site. For this mechanism,

$$A + B_i \underset{k_{off}(i)}{\overset{k_{on}(i)}{\rightleftharpoons}} C_i$$

where B_i and C_i denote the densities of different unoccupied and occupied surface site types, respectively. If the fraction of binding sites that are of each type is denoted by α_i, then the shape of the TIRFM binding curves (Figure 3) should be

$$F(A) = F(\infty)\sum_{i=1}^{n}\frac{\alpha_i A}{K_d(i) + A} \quad (23)$$

where n is the number of binding site types and

$$K_d(i) = \frac{k_{off}(i)}{k_{on}(i)} = \frac{AB_i}{C_i} \quad (24)$$

In the reaction limit, the fluorescence recovery curves should be of the shape shown in eq 1, i.e., eq 17 with

$$G(t) = \sum_{i=1}^{n}\alpha_i e^{-k_{off}(i)t} \quad (25)$$

Referring to the TIR/FPR data (Tables III and V), the data would imply, within this model of multiple binding site types, that the PS/POPC surfaces have three types of F-BF1 binding sites with approximately equivalent abundances α_i; and that two site types have measurable dissociation rates (≈ seconds) and one has a very slow dissociation rate (> minutes). However, to be consistent with the equilibrium binding data, which agrees well with the shape of eq 11, $K_d(1) \approx K_d(2) \approx K_d(3)$, which would imply that, referring to Table III, $k_{on}(1)/k_{on}(2) \approx k_{off}(1)/k_{off}(2) \approx 10$ and $k_{on}(3) \approx 0$. It is possible, although unlikely, that both the association and dissociation kinetic rates for each binding site type would change in such a way that the three dissociation constants were equal. However, the mechanism in which F-BF1 binds to different types of sites on PS/POPC surfaces is considered to be unlikely.

Multiple Conformations of Bound F-BF1. Another possibility is that the bound F-BF1 can assume more than one membrane-bound state. In this mechanism,

$$A + B \underset{k_{off}(1)}{\overset{k_{on}(1)}{\rightleftharpoons}} I \underset{k_{off}(2)}{\overset{k_{on}(2)}{\rightleftharpoons}} C$$

where I is an (perhaps loosely bound) intermediate, and

$$K_d(i) = \frac{k_{off}(i)}{k_{on}(i)} \quad (26)$$

where i = 1 or 2. For this mechanism, the equilibrium binding data would be of the shape

$$F(A) = \frac{F(\infty)A}{K_d(\text{app}) + A} \quad (27)$$

where

$$K_d(\text{app}) = \frac{K_d(1)K_d(2)}{1 + K_d(2)} \quad (28)$$

Equation 27 has the shape of eq 11 and therefore agrees with the data in Figure 3. In this mechanism, the values for K_d(app) equal those shown in Table II.

Neglecting the irreversible component of the fluorescence recovery, the reaction-limited TIR/FPR fluorescence recovery curves for this mechanism would be of the shape (Hsieh and Thompson, unpublished results)

$$G(t) = ge^{-\beta_1 t} + (1 - g)e^{-\beta_2 t} \quad (29)$$

where

$$g = \frac{[\beta_1 - \rho][k_{off}(1) - \beta_2]}{[\beta_1 - \beta_2][k_{off}(1) - \rho]} \quad (30)$$

$$2\beta_{1,2} = \rho \pm \sqrt{\rho^2 - 4k_{off}(1)k_{off}(2)} \quad (31)$$

$$\rho = k_{off}(1) + k_{on}(2) + k_{off}(2) \quad (32)$$

In this model, the measured TIR/FPR recovery rates k_1 and k_2 (Tables III and V) are equal to β_1 and β_2; and the fractional recovery associated with the first rate, i.e., $r_1/(r_1 + r_2)$ equals the constant g.

Algebraic manipulation of eqs 26, 28, and 30–32 shows that the measured apparent dissociation constants K_d (Table II) and kinetic parameters β_1, β_2, and g (Table V) may be used to calculate the kinetic rates and dissociation constants by using the following procedure: ρ is the sum of $\beta_1 + \beta_2$ (eq 31); $k_{off}(1)$, $k_{off}(2)$, and $k_{on}(2)$ are obtained by sequentially inverting eqs 30, 31, and 32, respectively; $K_d(2)$ is calculated from eq 26 (with i = 2); $K_d(1)$ is obtained by inverting eq 28; and $k_{on}(1)$ is then obtained from eq 26 (with i = 1). The kinetic and equilibrium parameters calculated by using this analysis on the data in Tables III and V are given in Table VI. As shown, most of the kinetic parameters are relatively independent of the PS concentration, *except for the initial membrane binding rate*, $k_{on}(1)$, which increases 12-fold between 5 and 25 mol % PS. Thus, in this model, the data imply that higher PS concentrations strongly affect the kinetics of the initial binding event but do not dramatically affect subsequent transitions between the two membrane-bound states.

Discussion

In the proenzyme activation reactions of the blood coagulation cascade, enzyme complex assembly on a membrane surface is an event crucial to the ultimate formation of a fibrin clot (Mann et al., 1990). Past studies have explored the equilibrium and kinetic properties of membrane binding by blood coagulation proteins using light scattering (Nelsestuen & Broderius, 1977; Nelsestuen & Lim, 1977; Wei et al., 1982), ellipsometry (Cuypers et al., 1983; Kop et al., 1984; Corsel

et al., 1986), and surface pressure monitoring (Mayer et al., 1983). In this work, two recently developed techniques in laser-based fluorescence microscopy (TIRFM and TIR/FPR) were used to directly measure the membrane equilibrium dissociation constants and kinetic dissociation rates of bovine prothrombin fragment 1 (BF1) at substrate-supported planar phospholipid membranes composed of mixtures of POPC and PS.

TIRFM measurements yielded an average dissociation constant of $K_d = 0.9$ μM for F-BF1 on membranes containing 25 mol % PS (Figure 3). This value agreed well with measurements made by the light scattering technique for both fluorescently labeled and unlabeled BF1 on small unilamellar vesicles (Figure 1). The measured value of K_d also agrees with previous literature reports for BF1 and prothrombin on vesicles, which range from 0.3 to 1.6 μM (Hermens et al., 1989; Mann et al., 1990; Dombrose et al., 1979), and for fluorescently labeled bovine prothrombin and its fragment 1 on planar model membranes (0.4 and 1 μM, respectively; Tendian et al., 1991). The measured dissociation constant for F-BF1 on planar membranes decreased when the amount of PS was increased (Table II), consistent with the equilibrium behavior of bovine prothrombin on small unilamellar vesicles (Wei et al., 1982; Kop et al., 1984). Thus, the use of TIRFM with substrate-supported, negatively charged planar membranes yields reasonable measurements of the membrane dissociation constants of BF1. The TIRFM measurements also gave an upper limit for the average area occupied by BF1 molecules at membrane saturation on 25 mol % PS planar membranes (3800 Å^2/molecule). This value is reasonably consistent with previous reports for BF1 and prothrombin on PS/POPC (50/50, mol/mol) small unilamellar vesicles (1800 Å^2/molecule; Lim et al., 1977) and on PS monolayers (1100 Å^2/molecule; Mayer et al., 1983).

TIR/FPR recovery curves for F-BF1 on PS-containing planar membranes gave average intrinsic dissociation kinetic rate constants of $k_{off}^a \approx 0.1$ s^{-1} (Tables III and V). The average intrinsic association kinetic rate constant for F-BF1 on PS/POPC planar membranes may thus be calculated from the measured values of k_{off}^a and K_d (Table II) as $k_{off}^a \approx 10^5$ M^{-1} s^{-1} (Table V). Two previous works have given prothrombin–membrane kinetic association and dissociation rate constants that are very different in magnitude; light scattering measurements of prothrombin binding to phospholipid vesicles have implied that $k_{on} \approx 10^7$ M^{-1} s^{-1} and $k_{off} \approx 3$ s^{-1} (Wei et al., 1982), whereas ellipsometry measurements of prothrombin binding to planar phospholipid bilayers have implied that $k_{on} \geq 3 \times 10^6$ M^{-1} s^{-1} and $k_{off} \geq 0.002$ s^{-1} (Corsel et al., 1986). Thus, the TIR/FPR value for k_{off}^a is within the reported range, but the value for k_{on}^a is much lower.

The TIR/FPR value for k_{on}^a as well as the values measured by other techniques (see above) are much lower than theoretical estimates of diffusion-limited association rate constants (Berg & von Hippel, 1985). A similar result has also recently been measured for epidermal growth factor at cell membranes (Hellen & Axelrod, 1991). Values of k_{on} that are much lower than the upper limit set by transport theory suggest that a large fraction of the collisional encounters between protein molecules in solution and the membrane surface do not result in successful membrane binding. The absence of a diffusion-limited intrinsic on-rate is not inconsistent with the observed diffusion-limited nature of the measured TIR/FPR fluorescence recovery curves at low F-BF1 solution concentrations, which is determined solely by the thickness of a slab adjacent to the membrane that contains a density of unbleached F-BF1 molecules equivalent to the surface density of bound F-BF1 (eqs 12 and 15).

The TIR/FPR fluorescence recovery curves for F-BF1 on PS/POPC membranes were nonmonoexponential. At F-BF1 solution concentrations <5 μM, this feature of the TIR/FPR recovery curves could be explained at least in part by the coupling between the intrinsic surface dissociation kinetics and transport in solution. However, the source of the nonmonoexponential behavior at high protein concentrations could not be attributed to diffusive phenomena. Thus, more complex binding mechanisms other than a simple reversible bimolecular reaction at the membrane surface were invoked. In general, more complex reaction mechanisms would result if multiple states existed for solution phase F-BF1, membrane-bound F-BF1, or F-BF1 membrane-binding sites. A model that is consistent with the TIR/FPR data is one in which bound F-BF1 exists in at least two states: a loose complex with $k_{off} \approx 0.3$ s^{-1} and a tighter complex with $k_{off} \approx 0.015$ s^{-1} (Table VI). Possible explanations for the different bound states include (1) heterogeneity arising from lateral interactions between membrane-bound F-BF1, (2) differences in the numbers of calcium ions that are simultaneously associated with F-BF1 and the membrane, (3) differences in the number of PS molecules that are associated with bound F-BF1, (4) a membrane-induced BF1 conformational change, or (5) different degrees of membrane penetration by nonpolar regions of F-BF1.

This work is the first application of TIR/FPR to the surface binding kinetics of a protein ligand at a planar phospholipid model membrane. The data demonstrate that this technique can yield quantitative kinetic data for protein–membrane association processes. The data also confirm an earlier theoretical treatment (Thompson et al., 1981) which predicts that TIR/FPR recovery curves may be limited either by the rate of solution transport or intrinsic surface dissociation and that the intrinsic rates will be measurable only above well-defined solution concentrations. Future TIR/FPR measurements should yield new information about membrane binding kinetics for other blood coagulation proteins or for these proteins in the presence of other membrane-bound enzymes and/or cofactors.

Acknowledgments

We thank ZhengPing Huang for preparing the Langmuir–Blodgett films and Pola Berkowitz for help with prothrombin fragment 1 preparations.

References

Axelrod, D., Burghardt, T. P., & Thompson, N. L. (1984) *Annu. Rev. Biophys. Bioeng. 13*, 247–268.

Bartlett, G. R. (1959) *J. Biol. Chem. 234*, 466–468.

Berg, O. G., & von Hippel, P. H. (1985) *Annu. Rev. Biophys. Bioeng. 14*, 131–160.

Bevers, E. M., Comfurius, P., van Rijn, J. L., Hemker, H. C. & Zwaal, R. F. A. (1982) *Eur. J. Biochem. 122*, 429–436.

Brian, A. A., & McConnell, H. M. (1984) *Proc. Natl. Acad. Sci. U.S.A. 81*, 6159–6163.

Burghardt, T. P., & Axelrod, D. (1981) *Biophys. J. 33*, 455–468.

Burghardt, T. P., & Thompson, N. L. (1984) *Biophys. J. 46*, 729–737.

Corsel, J. W., Willems, G. M., Kop, J. M. M., Cuypers, P. A., & Hermens, W. T. (1986) *J. Colloid Interface Sci. 111*, 544–554.

Cuypers, P. A., Corsel, J. W., Janssen, M. P., Kop, J. M. M., Hermens, W. T., & Hemker, H. C. (1983) *J. Biol. Chem. 258*, 2426–2431.

Dombrose, F. A., Gitel, S. N., Zawalich, K., & Jackson, C. M. (1979) *J. Biol. Chem. 254*, 5027–5040.
Furie, B., & Furie, B. C. (1988) *Cell 53*, 505–518.
Gemmell, C. H., Turrito, V. T., & Nemerson, Y. (1988) *Blood 72*, 1404–1406.
Habeeb, A. F. S. A. (1972) *Methods Enzymol. 25*, 457–464.
Hellen, E. H., & Axelrod, D. (1991) *J. Fluoresc. 1*, 113–128.
Hermens, W. T., Kop, J. M. M., & Willems, G. M. (1989) in *Coagulation and Lipids* (Zwaal, H. C., Ed.) pp 89–94, CRC Press, Inc., Boca Raton, FL.
Jackson, C. M., & Nemerson, Y. (1980) *Annu. Rev. Biochem. 49*, 765–811.
Kop, J. M. M., Cuypers, P. A., Lindhout, T., Hemker, H. C., & Hermens, W. T. (1984) *J. Biol. Chem. 259*, 13993–13998.
Lim, T. K., Bloomfield, V. A., & Nelsestuen, G. L. (1977) *Biochemistry 16*, 4177–4181.
Mann, K. G. (1977) *Methods Enzymol. 45*, 123–156.
Mann, K. G., Jenny, R. J., & Krishnaswamy, S. (1988) *Annu. Rev. Biochem. 57*, 915–956.
Mann, K. G., Nesheim, M. E., Church, W. R., Haley, P., & Krishnaswamy, S. (1990) *Blood 76*, 1–16.
Marsh, H. C., Scott, M. E., Hiskey, R. G., & Koehler, K. A. (1979) *Biochem. J. 183*, 513–517.
Mayer, L. D., Nelsestuen, G. L., & Brockman, H. L. (1983) *Biochemistry 22*, 316–321.
Mishell, B. B., & Shiigi, S. M. (1980) in *Selected Methods in Cellular Immunology*, pp 292–297 and 412–436, W. H. Freeman and Co., San Francisco, CA.
Nakache, M., Gaub, H. E., Schreiber, A. B., & McConnell, H. M. (1986) *Proc. Natl. Acad. Sci. U.S.A. 83*, 2874–2878.
Nelsestuen, G. L. (1976) *J. Biol. Chem. 251*, 5648–5656.
Nelsestuen, G. L., & Broderius, M. (1977) *Biochemistry 16*, 4172–4176.
Nelsestuen, G. L., & Lim, T. K. (1977) *Biochemistry 16*, 4164–4171.
Pisarchick, M. L., & Thompson, N. L. (1990) *Biophys. J. 58*, 1235–1249.
Poglitsch, C. L., & Thompson, N. L. (1990) *Biochemistry 29*, 248–254.
Poglitsch, C. L., Sumner, M. T., & Thompson, N. L. (1991) *Biochemistry 30*, 6662–6671.
Pollock, J. S., Shepard, A. J., Weber, D. J., Olson, D. L., Klapper, D. G., Pedersen, L. G., & Hiskey, R. G. (1988) *J. Biol. Chem. 263*, 14216–14223.
Prendergast, F. G., & Mann, K. G. (1977) *J. Biol. Chem. 252*, 840–850.
Reichert, W. M., Suci, P. A., Ives, J. T., & Andrade, J. D. (1987) *Appl. Spectrosc. 41*, 503–508.
Rosing, J., van Rijn, J. L., Bevers, E. M., van Dieijen, G., Comfurius, P., & Zwaal, R. F. A. (1985) *Blood 65*, 319–332.
Schmidt, C. F., Zimmerman, R. F., & Gaub, H. (1990) *Biophys. J. 57*, 577–588.
Schoen, P., Lindhout, T., Willems, G., & Hemker, H. C. (1990) *Thromb. Haemostasis 64*, 542–547.
Sheetz, M. P., & Koppel, D. E. (1979) *Proc. Natl. Acad. Sci. U.S.A. 76*, 3314–3317.
Smith, B. A., & McConnell, H. M. (1978) *Proc. Natl. Acad. Sci. U.S.A. 75*, 2759–2759.
Tendian, S. W., Lentz, B. R., & Thompson, N. L. (1991) *Biochemistry 30*, 10991–10999.
Thompson, N. L., Burghardt, T. P., & Axelrod, D. (1981) *Biophys. J. 33*, 435–454.
Thompson, N. L., Brian, A. A., & McConnell, H. M. (1984) *Biochim. Biophys. Acta 772*, 10–19.
Thompson, N. L., Palmer, A. G., Wright, L. L., & Scarborough, P. E. (1988) *Comments Mol. Cell. Biophys. 5*, 109–131.
Tilton, R. D., Gast, A. P., & Robertson, C. R. (1990a) *Biophys. J. 58*, 1321–1326.
Tilton, R. D., Robertson, C. R., & Gast, A. P. (1990b) *J. Colloid Interface Sci. 137*, 192–203.
Timbs, M. M., & Thompson, N. L. (1990) *Biophys. J. 58*, 413–428.
Watts, T. H., Brian, A. A., Kappler, J. W., Marrack, P., & McConnell, H. M. (1984) *Proc. Natl. Acad. Sci. U.S.A. 81*, 7564–7568.
Watts, T. H., Gaub, H. E., & McConnell, H. M. (1986) *Nature 320*, 179–181.
Weast, R. C., Ed. (1985) *CRC Handbook of Chemistry and Physics*, CRC Press, Boca Raton, FL.
Wei, G. J., Bloomfield, V. A., Resnick, R. M., & Nelsestuen, G. L. (1982) *Biochemistry 21*, 1949–1959.
Wright, L. L., Palmer, A. G., & Thompson, N. L. (1988) *Biophys. J. 54*, 463–470.
Zimmerman, R. M., Schmidt, C. F., & Gaub, H. E. (1990) *J. Colloid Interface Sci. 139*, 268–280.
Zot, H. G., Doberstein, S. K., & Pollard, T. D. (1992) *J. Cell Biol. 116*, 367–376.